

# Chaotic properties of spin lattices near second-order phase transitions

A. S. de Wijn,<sup>1,\*</sup> B. Hess,<sup>2</sup> and B. V. Fine<sup>2,3,4,†</sup>

<sup>1</sup>*Department of Physics, Stockholm University, 106 91 Stockholm, Sweden*

<sup>2</sup>*Institute for Theoretical Physics, University of Heidelberg, Philosophenweg 19, 69120 Heidelberg, Germany*

<sup>3</sup>*Department of Physics, School of Science and Technology,*

*Nazarbayev University 53 Kabanbai Batyr Ave., Astana 010000, Kazakhstan*

<sup>4</sup>*Skolkovo Institute of Science and Technology, 100 Novaya Str., Skolkovo, Moscow Region 143025, Russia*

We numerically investigate Lyapunov spectra of chaotic dynamics in lattices of classical spins in the vicinity of second-order ferromagnetic and antiferromagnetic phase transitions. On the basis of this investigation, we identify a characteristic of the shape of the Lyapunov spectra, which exhibits a sharp peak as a function of temperature exactly at the phase transition, provided the order parameter is capable of strong dynamic fluctuations. As a part of this work, we also propose a general numerical algorithm for determining the temperature in many-particle systems, where kinetic energy is not defined.

PACS numbers: 05.45.Jn, 75.10.Hk 75.30.Kz 05.20.-y 05.45.Pq 05.50.+q

The notion of chaos is often invoked in the context of the foundations of statistical physics in order to justify the ergodicity assumption, which is, in turn, used to derive the equilibrium Gibbs distribution. Beyond the above qualitative connection, the interplay between the quantitative characteristics of chaos and the statistical properties of many-particle systems still remains an elusive subject. In this paper, we present a detailed investigation of Lyapunov spectra as a function of temperature for lattices of classical spins with nearest-neighbor interaction in the vicinity of ferromagnetic (FM) and antiferromagnetic (AF) second-order phase transitions. We introduce a new characteristic of the shape of Lyapunov spectra, the “ $G$ -index”, which exhibits a sharp peak exactly at the phase transition temperature when the order parameter is capable of sufficiently strong dynamic fluctuations.

Most of the investigations of the temperature dependencies of Lyapunov instabilities in other systems have been limited so far to the largest Lyapunov exponents and often reported dramatic signatures of phase transitions [1–7]. The generality of these signatures, however, remains unclear. For some systems, these signatures may originate from the infinite range of particle-particle interactions [2, 7], while, for others, they may simply reflect the evolution of the phase space volume available to the system (see below). There exist only a limited number of investigations of entire Lyapunov spectra across phase transitions [8, 9]. So far, however, these investigations dealt only with first-order phase transitions. The present work builds on our earlier investigations of Lyapunov instabilities in classical spin lattices at infinite temperature [10, 11], where, in particular, we showed that the lattices are all chaotic with the exception of the Ising case.

We consider cubic lattices of  $N_s$  classical spins with periodic boundary conditions and the nearest-neighbor

interaction Hamiltonian:

$$\mathcal{H} = \sum_{i,j(i), i < j} J_x S_{ix} S_{jx} + J_y S_{iy} S_{jy} + J_z S_{iz} S_{jz}, \quad (1)$$

where  $(S_{ix}, S_{iy}, S_{iz}) \equiv \mathbf{S}_i$  are the three projections of the  $i$ th classical spin normalized by the condition  $\mathbf{S}_i^2 = 1$ , and  $J_x, J_y$  and  $J_z$  are the coupling constants, which we choose such that  $J_x^2 + J_y^2 + J_z^2 = 1$ . The notation  $j(i)$  indicates the nearest neighbors of the  $i$ -th spin.

Our procedure for computing the spectrum of Lyapunov exponents  $\{\lambda_i\}$  is described in Ref. [11]. It follows the standard approach of Ref. [12]. Index  $i$  in the above notation orders the Lyapunov exponents in the decreasing order with  $\lambda_1 \equiv \lambda_{\max}$  being the largest positive Lyapunov exponent. Due to the demanding nature of the numerical calculations of the full Lyapunov spectrum (order  $N_s^2$ ), we have had to restrict ourselves to lattices of  $8 \times 6 \times 4$ . For this system size, the finite-size effects on the Lyapunov exponents are already small [11, 13].

We numerically integrate the equations of motion associated with the Hamiltonian (1),  $\dot{\mathbf{S}}_i = \mathbf{S}_i \times \mathbf{h}_i$ , where  $\mathbf{h}_i = \sum_{j(i)} J_x S_{jx} \mathbf{e}_x + J_y S_{jy} \mathbf{e}_y + J_z S_{jz} \mathbf{e}_z$  is the local field. Here  $\mathbf{e}_x, \mathbf{e}_y$  and  $\mathbf{e}_z$  are orthogonal unit vectors. We use a fourth-order Runge-Kutta algorithm with time step 0.005 [16]. The initial conditions corresponding to a given value of the total energy of the system are selected using the routine described in Ref. [11].

The total energy  $E$  determines the temperature  $T$  of the system. However, this temperature cannot be found using the average kinetic energy per particle, because the notion of kinetic energy is not defined for spins. Below we describe a more general algorithm. It is applicable to any system with smooth dynamics and short-range interactions.

The algorithm is based on the definition  $1/T \equiv dS/dE$ , where  $S$  is the entropy of the system, which, is, in turn, defined (after setting  $k_B = 1$ ) as  $S \equiv \ln V(E)$ . Here  $V(E)$  is the  $(N - 1)$ -dimensional volume of the energy shell

in the  $N$ -dimensional many-particle phase space. The above definitions lead to  $\frac{1}{T} = \frac{1}{V(E)} \frac{dV(E)}{dE}$ , which implies that the volume of the energy shell changes nearly exponentially as a function of energy with the characteristic constant equal to the inverse temperature. Obtaining the above constant by random Monte-Carlo sampling of the entire many-particle phase space is not feasible. Instead, our algorithm consists of the following three steps: (i) It locates one point on any given energy shell using a dissipative dynamics routine introduced in Ref. [11]. (ii) It randomly samples that energy shell using sequential *energy-conserving* rotations of randomly chosen spins around the directions of their local fields by random angles. (iii) Finally, it explores the vicinity of each thus obtained point on the energy shell by tiny *energy non-conserving* rotations of each spin around a randomly chosen axis perpendicular to spin's direction. The small angles for these rotations are drawn from a Gaussian distribution around zero. (For the lattices considered, we used a standard deviation of 0.014 rad.) Since  $V(E)$  grows exponentially with energy, an energy increase as a result of step (iii) is more likely than an energy decrease. We recover the value of temperature by first obtaining the mean and the mean-squared changes of energy,  $\langle \Delta E \rangle$  and  $\langle \Delta E^2 \rangle$  respectively, and then substituting them into the formula

$$T = \frac{\langle \Delta E^2 \rangle}{2\langle \Delta E \rangle}, \quad (2)$$

which is derived in the supplement [13].

After obtaining the energy-temperature relation, we find the specific heat from  $C(T) = dE/dT$ . In the thermodynamic limit,  $C(T)$  exhibits a jump at the temperatures of the FM and AF phase transitions, but, for finite-size lattices, the jumps of  $C(T)$  are not perfectly vertical. Therefore, we identify the phase transition temperature  $T_c$  as the temperature of the steepest change of  $C(T)$ .

In our systems,  $E = 0$  corresponds to infinite temperature, while  $E < 0$  and  $E > 0$  correspond to positive and negative temperatures respectively. Because cubic spin lattices with nearest-neighbor interactions are bipartite,  $V(E) = V(-E)$  (see [13]). As a result, an AF transition at temperature  $T_c$  implies an FM transition at temperature  $-T_c$ . We define the order parameters as  $\phi = \left| \frac{1}{N_s} \sum_i (\pm 1) \mathbf{S}_i \right|$ , where the FM order implies all signs  $+1$ , while the AF order implies  $+1$  and  $-1$  alternating between adjacent lattice sites.

Despite the above mentioned symmetry of  $V(E)$ , the Lyapunov spectra are, in general, not symmetric with respect of  $E = 0$ , with the exception of the  $XX$ -interaction characterized by  $J_x = J_y \neq 0$  and  $J_z = 0$  [13].

We now turn to the results of our simulations for the case of the Heisenberg interaction  $J_x = J_y = J_z = 1/\sqrt{3}$  at positive temperatures. Figure 1 shows the energy and temperature dependences of the largest Lyapunov expo-

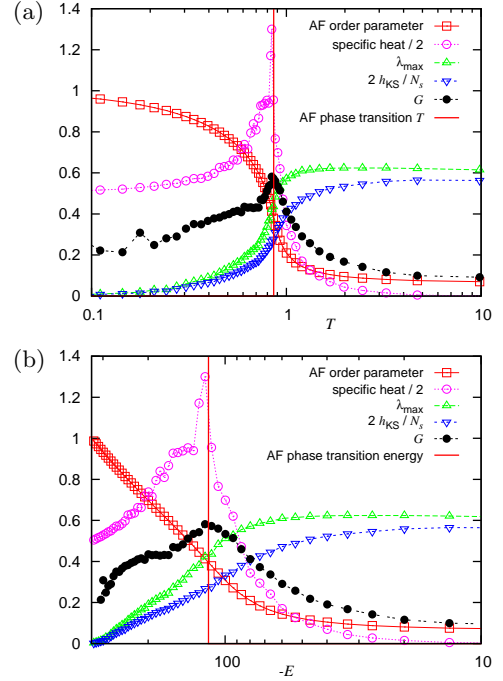


FIG. 1: Specific heat, AF order parameter, the largest Lyapunov exponent, Kolmogorov-Sinai entropy and the  $G$ -index as functions of (a) temperature and (b) energy for the  $8 \times 6 \times 4$  lattice with Heisenberg interaction  $J_x = J_y = J_z = 1/\sqrt{3}$ . The positions of the AF phase transition are indicated by the vertical lines.

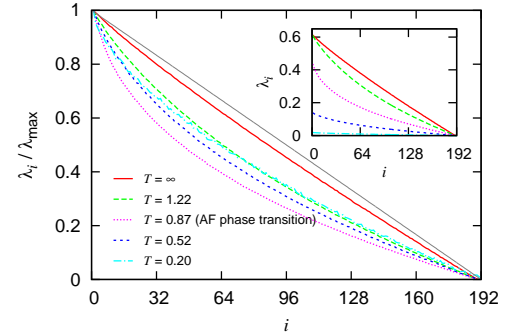


FIG. 2: Examples of Lyapunov spectra for the lattice used for Fig. 1. The thin gray straight line extending along the diagonal of the main plot is drawn to illustrate the geometrical interpretation of the  $G$ -index given in the text.

nent  $\lambda_{\max}$  and the Kolmogorov-Sinai entropy  $h_{\text{KS}}$  (equal to the sum of all positive Lyapunov exponents) together with the specific heat and the order parameter. Corresponding examples of complete Lyapunov spectra are presented in Fig. 2.

Comparing Figs. 1 (a) and (b), we observe that both  $\lambda_{\max}$  and  $h_{\text{KS}}$  exhibit a steep change across the AF phase transition as functions of temperature but not as functions of energy. In general, such behavior is expected for any smooth function of energy  $f(E)$ , which is then con-

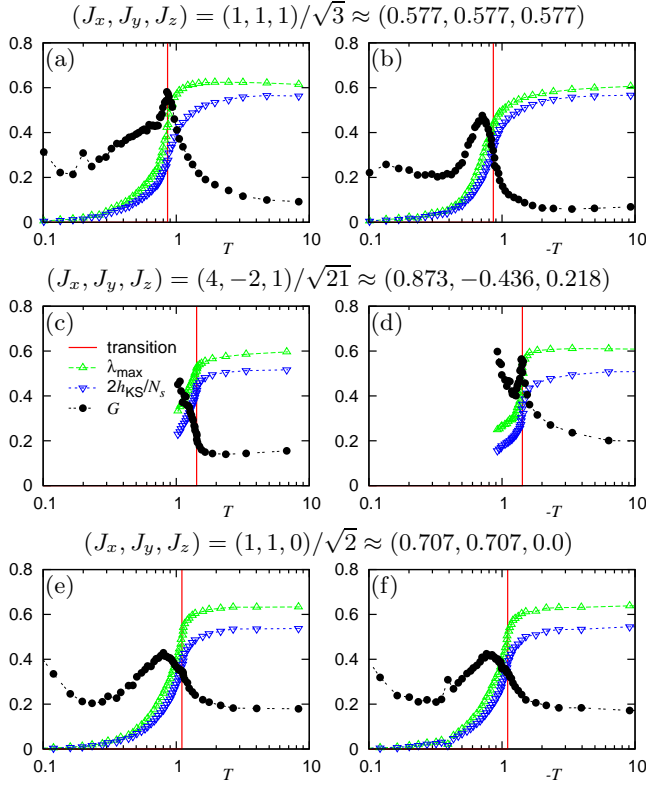


FIG. 3: Indicators of the phase transition and dynamic quantities as a function of temperature, for Heisenberg coupling and two types of anisotropic coupling. The coupling constants are indicated above the plots. Both the AF and the FM sides are shown. Below some transitions, formation of magnetic domains prevents the averages and Lyapunov exponents from converging sufficiently within the simulation time.

verted to a function of temperature  $\tilde{f}(T) \equiv f(E(T))$ . For the latter function,  $d\tilde{f}/dT = \frac{df}{dE} \frac{dE}{dT} = \frac{df}{dE} C(T)$ . Since  $C(T)$  exhibits a jump at the phase transition, so does  $d\tilde{f}/dT$ . In other words, the steep changes of  $\lambda_{\max}(T)$  and  $h_{\text{KS}}(T)$  around  $T = T_c$  as such indicate only the change of the energy-temperature relation rather than an intrinsic sensitivity of Lyapunov instabilities to phase transitions.

The examples of spectra shown in Fig. 2, nevertheless indicate that the phase transition influences the shape of the Lyapunov spectra: the closer the temperature to  $T_c$ , the more curved the spectrum. We quantify this shape change by a simple ratio, which we call the “ $G$ -index”:

$$G = \frac{N\lambda_{\max}}{2h_{\text{KS}}} - 1. \quad (3)$$

It represents the total area between the spectrum and the diagonal line extending in Fig. 2 from  $(0, 1)$  to  $(N_s, 0)$ , divided by the area under the spectrum. The  $G$ -index is plotted in Fig. 1. It exhibits a sharp peak at the phase transition as a function of temperature and also a clear maximum at the corresponding energy.

Motivated by the above finding, we have systematically

investigated the  $G$ -index for other interaction parameters. Fig. 3 presents  $\lambda_{\max}$ ,  $h_{\text{KS}}$  and  $G$  at positive and negative temperatures for the Heisenberg interaction [(a) and (b)], generic anisotropic interaction [(c) and (d)] and the  $XX$ -interaction [(e) and (f)]. The AF transitions in all three cases occurred at positive temperatures, while the FM transitions occurred at negative temperatures. Typically, as shown in Figs. 3 (a)–(d)  $G(T)$  exhibited a sharp peak at either FM or AF phase transitions but never at both. The  $XX$ -interaction was the only case where we observed no peak of  $G(T)$  at either phase transition.

The behavior of  $G(T)$  away from the phase transition, in particular the appearance of humps of  $G(T)$  in Figs. 3 (b), (f), and (e), may also be of interest, but it extends beyond the scope of the present work. Here we only remark that our calculations far into the ordered phases for generic anisotropic couplings of the type presented in Fig. 3 (c) and (d) exhibited very slow convergence — probably because of the formation of magnetic domains.

Now we turn to explaining the presence or the absence of the peaks of  $G(T)$  at  $T = T_c$ . In general, all positive Lyapunov exponents tend to decrease with decreasing  $|T|$ , because the phase space volume available to the system becomes smaller. The function  $G(T)$  given by Eq. (3) is sensitive to the difference between the temperature dependences of  $\lambda_{\max}$  and the average positive Lyapunov exponent  $\lambda_{\text{av}} \equiv h_{\text{KS}}/N_s$ .

Let us follow the behavior of  $G(T)$  starting from infinite temperature and then decreasing  $|T|$ . As can be seen in Figs. 3 (a) and (d),  $G(T)$  exhibits a peak at  $T = T_c$  when  $\lambda_{\max}$  initially decreases more slowly than  $\lambda_{\text{av}}$  and then drops faster around  $T = T_c$ , thereby catching up with  $\lambda_{\text{av}}$ . We now propose an argument, which we later substantiate by examples, that the above behavior of  $\lambda_{\max}$  is due to the fact that the order parameter is capable of strong dynamical fluctuations. In such a case, the Lyapunov vector corresponding to  $\lambda_{\max}$  seeks the directions in the phase space corresponding to the faster-than-average dynamics, which are, in turn, correlated with the combinations of variables contributing to  $\phi$ .

In the opposite case, when  $\phi$  is not capable of sufficiently strong dynamical fluctuations, the Lyapunov vector corresponding to  $\lambda_{\max}$  ignores the respective directions in the phase space. In such a case,  $\lambda_{\max}(T)$  and  $\lambda_{\text{av}}(T)$  exhibit very similar behavior over the entire range of temperatures seen in Figs. 3 (b), (c), (e) and (f), and, as a result,  $G(T)$  does not have a peak at  $T = T_c$ .

In order to exemplify the notion of strong dynamical fluctuations of the order parameter, let us assume that the magnetic order sets in along the  $x$ -axis. [This is the only possible direction for the interaction used for Figs. 3 (c) and (d), or one of a continuous set of possible directions for Figs. 3 (a), (b), (e) and (f).] Let us then

decompose the Hamiltonian as

$$\mathcal{H} = \sum_{m,n(m),m<n} \left[ \frac{1}{4}(J_y - J_z)(S_{m+}S_{n+} + S_{m-}S_{n-}) + \frac{1}{4}(J_y + J_z)(S_{m+}S_{n-} + S_{m-}S_{n+}) + J_x S_{mx}S_{nx} \right], \quad (4)$$

where we use spin raising and lowering variables  $S_{m+} = S_{my} + iS_{mz}$  and  $S_{m-} = S_{my} - iS_{mz}$ , which are analogous to the raising and lowering quantum spin operators and have the same interpretations as far as the local dynamical trends are concerned [14, 15]. We refer to the first two terms in the right-hand-side of Eq. (4) as “double-flip” and “flip-flop” terms respectively. The first of them changes the  $z$ -projections of the two spins in the same direction, while the second one changes them in the opposite directions. The flip-flop term makes AF order fluctuate, while conserving the FM order. The double-flip term has the opposite effect.

For the Heisenberg Hamiltonian,  $J_y = J_z$ . Therefore, the double-flip term is zero, while the flip-flop term dominates. As a result, the AF order strongly fluctuates in time near the phase transition, which, according to our argument, leads to the peak of  $G(T)$  seen in Fig. 3 (a). On the contrary, the FM order that sets in for the same Hamiltonian at negative temperatures does not fluctuate in time. Accordingly,  $G(T)$  does not exhibit a peak at  $T = T_c$  in Fig. 3 (b).

For the anisotropic interaction corresponding to Figs. 3 (c) and (d),  $|J_y - J_z| > |J_y + J_z|$ . Therefore, the double-flip term in the Hamiltonian dominates. This leads to the peak of  $G(T)$  at the FM transition and no peak at the AF transition.

For the XX-interaction corresponding to Figs. 3 (e) and (d),  $|J_y - J_z| = |J_y + J_z|$ . Therefore, the flip-flop and the double-flip terms have equal strength, which implies that the Lyapunov vector corresponding to  $\lambda_{\max}$  does not particularly seek either FM or AF correlations. As a result, there are no peaks of  $G(T)$  at either FM transition or AF transition.

The above interpretation is supported by our Fourier analysis of the components of Lyapunov vectors  $\{\delta\mathbf{S}_{(n_x, n_y, n_z)}\}$  [11]. Here  $(n_x, n_y, n_z)$  are the cubic lattice indices. We compute the function  $F(k_x, k_y, k_z) \equiv \mathbf{A}^*(k_x, k_y, k_z) \cdot \mathbf{A}(k_x, k_y, k_z)$ , where

$$\mathbf{A}(k_x, k_y, k_z) \equiv \sum_{n_x, n_y, n_z} \delta\mathbf{S}_{(n_x, n_y, n_z)} e^{-i(k_x n_x + k_y n_y + k_z n_z)}, \quad (5)$$

and  $(k_x, k_y, k_z)$  are the wave numbers of the discrete Fourier components.

$F(k_x, k_y, k_z)$  for the Heisenberg case is presented in Fig. 4. The left column of this figure shows  $F(k_x, k_y, k_z)$  for the Lyapunov vector corresponding to  $\lambda_{\max}$  at the temperature of the AF phase transition. For comparison,

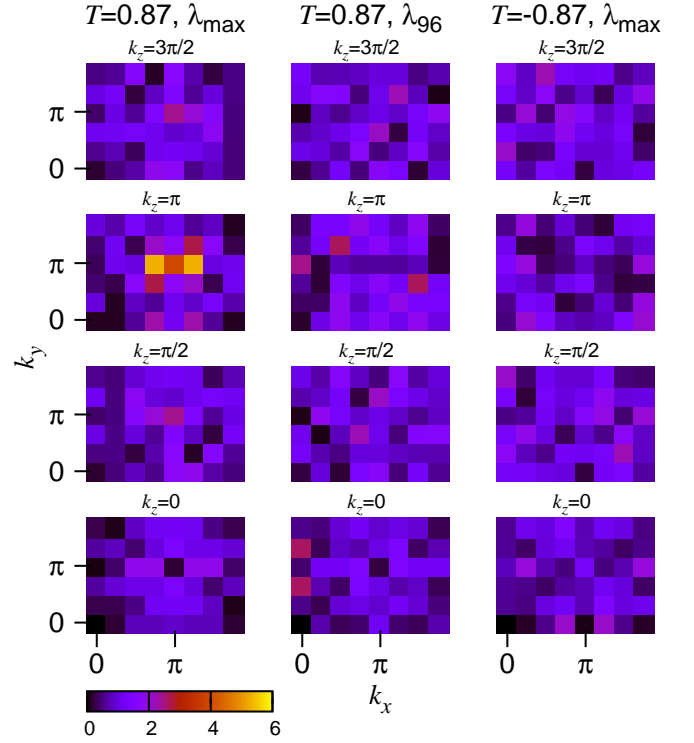


FIG. 4: Spectral functions  $F(k_x, k_y, k_z)$  of three Lyapunov vectors for the lattice with Heisenberg interaction used for Figs. 3 (a) and (b). The left and the middle columns of frames represent  $F(k_x, k_y, k_z)$  for the Lyapunov vectors corresponding to  $\lambda_{\max}$  and  $\lambda_{96}$ , respectively, at the AF transition temperature. The right column corresponds to the Lyapunov vector for  $\lambda_{\max}$  at the FM transition temperature. Each column shows a complete set values of  $F(k_x, k_y, k_z)$  encoded as color pixels: one pixel for each of  $8 \times 6 \times 4$  possible combinations of wave numbers  $(k_x, k_y, k_z)$ . Each frame contains  $8 \times 6$  pixels for a fixed value of  $k_z$  indicated above the frame.

the middle column represents  $F(k_x, k_y, k_z)$  for the Lyapunov exponent  $\lambda_{96}$  taken from the middle of the positive side of the Lyapunov spectrum at the same temperature and the right column corresponds to  $\lambda_{\max}$  but at the (negative) temperature of the FM transition. In the first case, the bright spots in Fig. 4 around  $k_x = k_y = k_z = \pi$  indicate strong AF correlations. In the later two cases, no correlations of AF or FM type are apparent.

To summarize, we have identified a characteristics of Lyapunov spectra of many-spin systems — the  $G$ -index — which, as a function of temperature exhibits a clear peak at magnetic phase transitions, provided the variable associated with the order parameter is capable of strong dynamic fluctuations. We expect similar behavior near second-order phase transitions in other many-particle systems with short-range interactions.

The authors are grateful to T. A. Elsayed for helpful discussions during the initial stage of this work. A.S.dW’s work is financially supported by an Unga Forskare grant from the Swedish Research Council. The

numerical part of this work was performed at the bw-GRiD computing cluster at the University of Heidelberg.

---

\* Electronic address: `dewijn@fysik.su.se`

† Electronic address: `B.Fine@thphys.uni-heidelberg.de`

- [1] L. Caiani, L. Casetti, C. Clementi, and M. Pettini, *Phys. Rev. Lett.* **79**, 4361 (1997).
- [2] V. Latora, A. Rapisarda, and S. Ruffo, *Phys. Rev. Lett.* **80**, 692 (1998).
- [3] L. Casetti, M. Cerruti-Sola, M. Modugno, G. Pettini, M. Pettini, and R. Gatto, *Rivista del Nuovo Cimento* **22** (1999).
- [4] J. Barr and T. Dauxois, *EPL (Europhysics Letters)* **55**, 164 (2001).
- [5] K.-H. Kwon and B.-Y. Park, *J. Chem. Phys.* **107**, 5171 (1997).
- [6] M. Cerruti-Sola, C. Clementi, and M. Pettini, *Phys. Rev. E* **61**, 5171 (2000).
- [7] M.-C. Firpo, *Phys. Rev. E* **57**, 6599 (1998).
- [8] C. Dellago and H. A. Posch, *Physica A* **230**, 364 (1996).
- [9] H. Bosetti and H. A. Posch, *Communications in Theoretical Physics* **62**, 451 (2014).
- [10] A. S. de Wijn, B. Hess, and B. V. Fine, *Phys. Rev. Lett.* **109**, 034101 (2012).
- [11] A. S. de Wijn, B. Hess, and B. V. Fine, *Journal of Physics A: Mathematical and Theoretical* **46**, 254012 (2013).
- [12] G. Benettin, L. Galgani, A. Giorgilli, and J. M. Strelcyn, *Meccanica* **15**, 9 (1980).
- [13] See EPAPS supplemental material for the derivation of Eq.(5), discussion of the symmetry of various quantities with respect to changing the sign of energy  $E$ , plots illustrating finite-size effects, additional plots of the type presented in Figs. 2 and 3.
- [14] B. V. Fine, *Phys. Rev. Lett.* **79**, 4673 (1997).
- [15] B. V. Fine, *Int. J. Mod. Phys. B* **18**, 1119 (2004).
- [16] During the time of our simulations, typically equal to 20000, the total energy is conserved with absolute accuracy better than  $10^{-6}$ .

**Supplemental material for the  
manuscript “Chaotic properties of  
classical spin lattices near second-order  
phase transitions”**

A. S. de Wijn, B. Hess, and B. V. Fine

**FINDING TEMPERATURE ASSOCIATED WITH  
A GIVEN ENERGY SHELL**

Here we derive Eq. (2) of the main article by perturbing an energy shell and making use of the fact that

$$\frac{1}{T} = \frac{1}{V(E)} \frac{dV(E)}{dE}. \quad (\text{S1})$$

Let us start by mentioning that an intuitive insight in the forthcoming general derivation can be gained by considering an example of  $N$ -dimensional Euclidean phase space, and assuming that the energy is given by the distance to the origin of a cartesian coordinate system in this space. In this case the family of the energy shells becomes a continuous set of  $(N - 1)$ -dimensional hyperspherical surfaces with a common center.

Turning to the general case, let us denote the complete set of coordinates in  $N$ -dimensional many-particle phase space as  $\{q_1, \dots, q_N\} \equiv \mathbf{q}$ . An energy shell corresponding to energy  $E_0$  is defined by condition

$$E(\mathbf{q}) = E_0. \quad (\text{S2})$$

The corresponding  $(N - 1)$ -dimensional phase space volume is  $V(E_0)$ . Let us further consider a small element of volume  $\delta V(E_0)$  on this energy shell. If the energy changes by value  $dE$ , the above element can be bijectively mapped onto an element of the new energy shell by moving in the direction orthogonal to the original energy shell. The change of the coordinates in this case is

$$\mathbf{q} \rightarrow \mathbf{q} + d\mathbf{q}, \quad (\text{S3})$$

where

$$d\mathbf{q} = \mathbf{g} \frac{dE}{|\mathbf{g}|^2}. \quad (\text{S4})$$

Here  $\mathbf{g} \equiv \partial E(\mathbf{q})/\partial \mathbf{q}$  is the vector orthogonal to the original energy shell at a given point. The individual components of this vector are  $g_i = \partial E(q_1, \dots, q_N)/\partial q_i$ . The volume of the above element of the energy surface after transformation (S3) is

$$\delta V(E_0 + dE) = \delta V(E_0) \det \left[ \delta_{ij} + dE \frac{\partial}{\partial q_i} \left( \frac{g_j}{|\mathbf{g}|^2} \right) \right], \quad (\text{S5})$$

where  $\delta_{ij}$  is the Kronecker delta. Strictly speaking, the determinant in Eq. (S5) represents the growth of an  $N$ -dimensional rather than  $(N - 1)$  dimensional volume element, because it includes the energy direction itself. However, since this is only one of  $N \gg 1$  directions, the error in the final result associated with the above approximation is of the order of  $1/N$ . Now, we write explicitly

$$\begin{aligned} \frac{\partial}{\partial q_i} \left( \frac{g_j}{|\mathbf{g}|^2} \right) &= \frac{1}{|\mathbf{g}|^2} \frac{\partial^2 E}{\partial q_i \partial q_j} \\ &- \frac{1}{|\mathbf{g}|^4} \frac{\partial E}{\partial q_j} \frac{\partial}{\partial q_i} \left[ \left( \frac{\partial E}{\partial q_1} \right)^2 + \dots + \left( \frac{\partial E}{\partial q_N} \right)^2 \right], \end{aligned} \quad (\text{S6})$$

and then observe that for a system with short-range interactions, the first term in the above equation is of the order of  $1/N$ , while the second term is of the order of  $1/N^2$  and hence can be neglected. We further notice that the leading (first-order) contributions to the determinant in Eq. (S5) in terms of  $dE$  come only from the diagonal elements of the matrix. Taking into account the above two considerations, we finally obtain that, in the limit  $N \rightarrow \infty$ ,

$$\delta V(E_0 + dE) = \delta V(E_0) \left( 1 + \frac{\mathcal{K}}{|\mathbf{g}|^2} dE \right), \quad (\text{S7})$$

where  $\mathcal{K} = \sum_i \partial^2 E / \partial q_i^2$ . The total change of the volume of the energy shell is then

$$V(E_0 + dE) = V(E_0) \left( 1 + \left\langle \frac{\mathcal{K}}{|\mathbf{g}|^2} \right\rangle dE \right), \quad (\text{S8})$$

where the notation  $\langle \dots \rangle$  implies the average of the entire energy shell.

Eq. (S8) together with Eq. (S1) implies that  $1/T = \langle \mathcal{K}/|\mathbf{g}|^2 \rangle$ . Since both  $|\mathbf{g}|^2$  and  $\mathcal{K}$  contain additive small contributions associated with the uncorrelated remote parts of a large system, the distributions for each of them are narrowly peaked around the respective average values (according to the central limit theorem). Therefore, in the limit  $N \rightarrow \infty$ ,

$$\frac{1}{T} = \frac{\langle \mathcal{K} \rangle}{\langle |\mathbf{g}|^2 \rangle}. \quad (\text{S9})$$

In our simulations, both  $\langle \mathcal{K} \rangle$  and  $\langle |\mathbf{g}|^2 \rangle$  are obtained from the perturbations of the phase space vector  $\Delta \mathbf{q}$  associated with the small random spin rotations introduced in the main article and characterized by mean-squared values  $\sigma_q^2 \equiv \langle \Delta q_i^2 \rangle \ll 1/N$ . These perturbations are schematically illustrated in Fig. S1. The energy change for each perturbation is

$$\Delta E \approx \sum_i g_i \Delta q_i + \frac{1}{2} \sum_{i,j} \frac{\partial^2 E}{\partial q_i \partial q_j} \Delta q_i \Delta q_j, \quad (\text{S10})$$

from which it follows that, in the limit  $\sigma_q^2 \rightarrow 0$ ,  $\langle \Delta E \rangle = \frac{1}{2} \langle \mathcal{K} \rangle \sigma_q^2$ , while  $\langle \Delta E^2 \rangle = \langle |\mathbf{g}|^2 \rangle \sigma_q^2$ . Substituting the later two formulas into Eq. (S9), we obtain Eq. (2) of the main article.

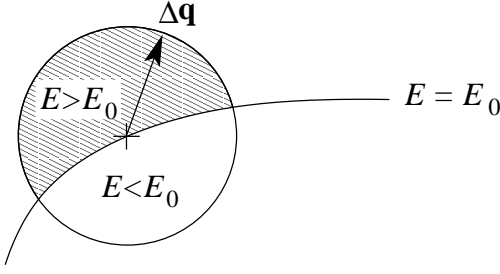


FIG. S1: A diagram illustrating how a point on an energy shell becomes displaced by a perturbation  $d\mathbf{q}$  that changes the energy. Due to the curvature of the energy shell, an increase in the energy is more likely than a decrease (for  $T > 0$ ).

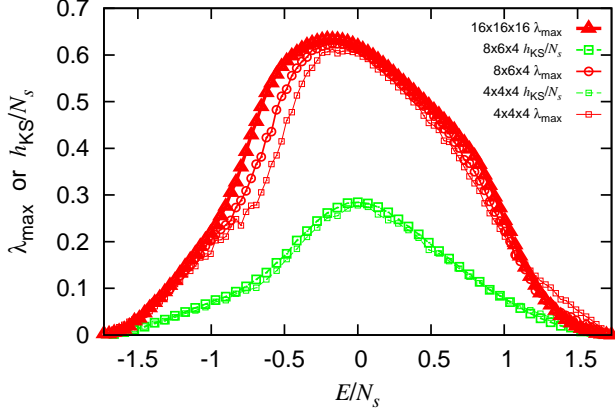


FIG. S2: The largest Lyapunov exponent and Kolmogorov-Sinai entropy per spin for several different lattice sizes as functions of the energy per spin. The Kolmogorov-Sinai entropy for the  $16 \times 16 \times 16$  system is not shown, as it is impossible to obtain sufficiently accurately with currently available computing power.

### SYMMETRY BETWEEN POSITIVE AND NEGATIVE ENERGIES

Cubic spin lattices with nearest-neighbor interactions are bipartite, in the sense that they can be divided into two sublattices such that spins of one sublattice interact only with the spins of the other sublattice. The reversal of all spin coordinates for one sublattice changes the sign of  $E$  while leaving the volume of the corresponding phase space elements the same. As a result, the volumes of energy shells  $V(E)$  are symmetric with respect to  $E = 0$  corresponding to the infinite temperature. The above symmetry of  $V(E)$  implies that, if an antiferromagnetic transition occurs at temperature  $T_c$ , then, in the same system, a ferromagnetic transition occurs at temperature  $-T_c$ .

Despite the above symmetry of  $V(E)$ , the Lyapunov

spectra are, in general, not symmetric with respect of  $E = 0$ , because the reversal of all three projections of a spin does not preserve Poisson brackets for spin projections (see Ref. [11]) and hence changes the character of the dynamics. The only symmetric case is the  $XX$ -interaction characterized by  $J_x = J_y \neq 0$  and  $J_z = 0$ . In this case, one can reverse only  $x$ - and  $y$ -components for the spins of one of the two sublattices without reversing their  $z$ -components, thereby protecting the Poisson brackets and, at the same time, reversing the energy.

### FINITE-SIZE EFFECTS

Here we include Fig. S2 illustrating the size-dependence of the largest Lyapunov exponent and the Kolmogorov-Sinai entropy.

### ADDITIONAL PLOTS

Figure S3 shows plots similar to Fig. 3 but for different anisotropic couplings. Here in particular the comparison of Fig. S3 (c) with Fig. 3 (d), and Fig. S3 (d) with Fig. 3 (c) demonstrate the symmetry of Lyapunov spectra of bipartite spin lattices with respect to the simultaneous sign reversals of the total energy and of one of the coupling constants. Finally, in Fig. S4, we also present the Lyapunov spectra for anisotropic coupling used for Figs. S3 (c) and (d) of the main article.

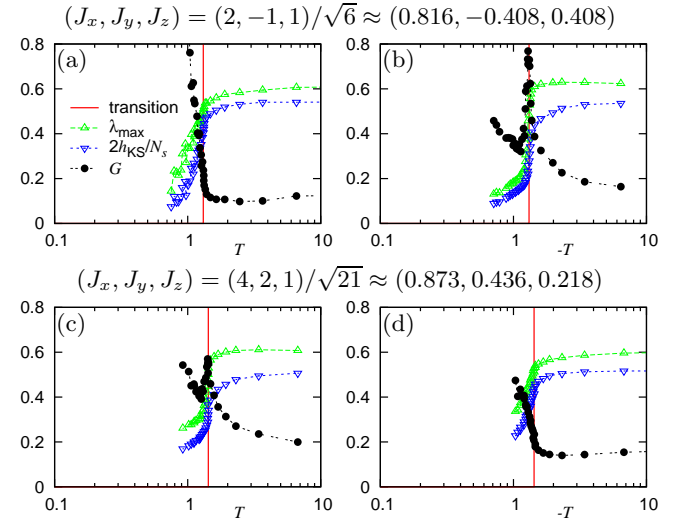


FIG. S3: Lyapunov exponents and  $G$ -index as functions of temperature for several different sets of coupling constants (indicated above the plots). The position of the phase transition is indicated with a red vertical line.

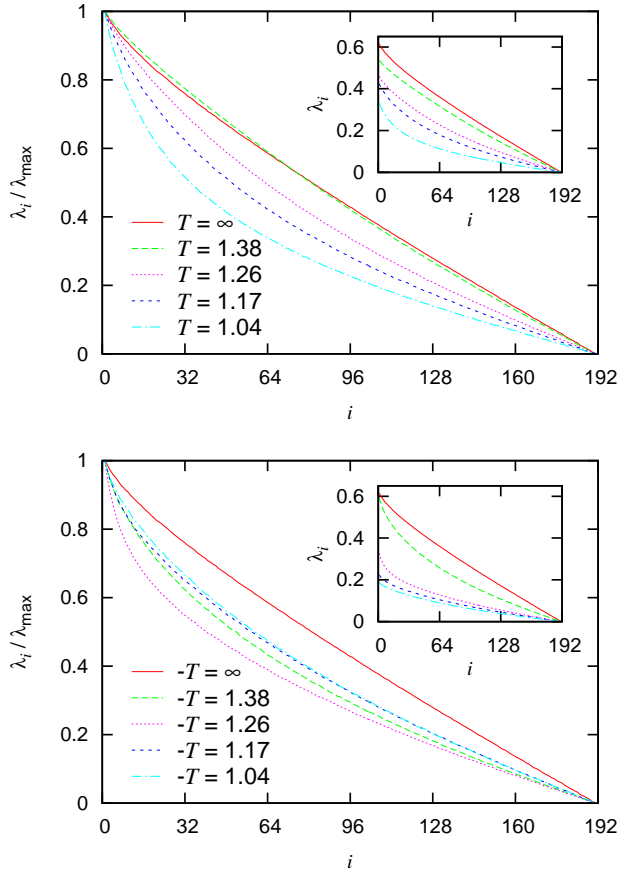


FIG. S4: Rescaled Lyapunov spectra for different temperatures above and below the phase transition, for  $(J_x, J_y, J_z) = (2, -1, 1)/\sqrt{6} \approx (0.816, -0.408, 0.408)$  [Fig. 3 (c) and (d) of the main article] with system size  $8 \times 6 \times 4$ . The insets show the unrescaled spectra. The maximum curvature of the spectrum appears only at the transition at negative temperatures.